JOURNAL OF GUIDANCE, CONTROL, AND DYNAMICS
Vol. 31, No. 1, January–February 2008

Engineering Notes

ENGINEERING NOTES are short manuscripts describing new developments or important results of a preliminary nature. These Notes should not exceed 2500 words (where a figure or table counts as 200 words). Following informal review by the Editors, they may be published within a few months of the date of receipt. Style requirements are the same as for regular contributions (see inside back cover).

Attitude Dynamics of Rigid Bodies in the Vicinity of Lagrangian Points

Brian Wong,* Rakesh Patil,† and Arun Misra‡
McGill University,
Montreal, Quebec H3A 2K6, Canada

DOI: 10.2514/1.28844

I. Introduction

IN THE last 30 years, several sun-monitoring spacecraft have orbited around the sun–Earth L_1 point, and several space observatories will be placed near the sun–Earth L_2 in the next decade. Although a large body of literature exists on the orbital dynamics of spacecraft in the restricted three-body problem, very few have explored the attitude dynamics of a rigid Lagrangian-point spacecraft. Kane and Marsh [1] considered the attitude dynamics of an axial symmetric satellite that is rotating about its axis of symmetry, which is normal to the primary bodies' orbital plane. Robinson [2] first studied the attitude dynamics of a dumbbell satellite located at a triangular point. The same author [3] later determined the equilibrium attitudes of an arbitrary shaped satellite located at a collinear point or at a triangular point and constructed a linear stability diagram about one of the equilibrium configurations. Misra and Bellerose [4] studied the librational dynamics of a tethered satellite located at the Earth–moon Lagrangian points and obtained the libration frequencies. The rigid spacecraft is assumed to be held at the Lagrangian points in all of these studies. In practice, however, collinear point satellites are not located directly at the Lagrangian point but in periodic orbits around the point. This note extends the work done by Robinson [3] and Misra and Bellerose [4] and addresses the question of how the translational motions of the spacecraft affect its attitude dynamics. The attitude dynamics of the satellite are studied while it is in a planar Lyapunov orbit and its three-dimensional counterpart. A triangular point spacecraft was previously demonstrated to have two equilibrium configurations, and linear stability diagrams about both equilibrium configurations for a L_4 spacecraft are also presented.

Presented as Paper 6653 at the AIAA/AAS Astrodynamics Specialist Conference and Exhibit, Keystone, Colorado, 21–24 August 2006; received 13 November 2006; revision received 10 July 2007; accepted for publication 16 July 2007.

*Graduate Assistant, Department of Mechanical Engineering, 817 Sherbrooke Street West, Room MD350.

†Summer Intern, Department of Mechanical Engineering, 817 Sherbrooke Street West, Room MD350.

‡Professor, Department of Mechanical Engineering, 817 Sherbrooke Street West. Fellow AIAA.

II. Problem Formulation

A finite-size rigid spacecraft of mass m is set in a circular restricted three-body problem (Fig. 1), replacing the small point mass in the classical setup. The dimensions of the spacecraft are negligibly small compared with the distance between the primary bodies. The two primary masses, M_1 and M_2, are assumed to revolve around their common center of mass O in circular orbits. The variable D denotes the distance between the primary bodies, while D_1 and D_2 denote the distance of M_1 and M_2 from O, respectively.

The orbital motion of the spacecraft is described using a rotating orbital frame $[\ x \quad y \quad z]$, with its origin at O and the x axis points from M_1 to M_2. The z axis is parallel to the angular momentum vector of the primary bodies, and the y axis completes the triad. Unit vectors along the x, y, and z axes are denoted by $\mathbf{i}$, $\mathbf{j}$, and $\mathbf{k}$, respectively. The axes rotate about the z axis with the angular rate of Ω, where $\Omega = [G(M_1 + M_2)/D^3]^{1/2}$ and G denotes the universal gravitational constant. The position vectors of the center of mass of the spacecraft, relative to the Lagrangian point of interest, M_1, and M_2, respectively, can be written as

$$\mathbf{R}_p = x_p\mathbf{i} + y_p\mathbf{j} + z_p\mathbf{k} \tag{1}$$

$$\mathbf{R}_1 = (D_1 + X_L + x_p)\mathbf{i} + (Y_L + y_p)\mathbf{j} + z_p\mathbf{k} \tag{2}$$

$$\mathbf{R}_2 = (-D_2 + X_L + x_p)\mathbf{i} + (Y_L + y_p)\mathbf{j} + z_p\mathbf{k} \tag{3}$$

where $(X_L, Y_L, 0)$ are the coordinates of the Lagrangian point and x_p, y_p, and z_p are measured from there. The body reference frame $[x_B\ y_B\ z_B]$, aligned with the principal axes of the body and with unit vectors $\mathbf{i}_B$, $\mathbf{j}_B$, and $\mathbf{k}_B$, is attached to the center of mass of the rigid body. The relationship between the body frame with respect to the orbital frame is described in terms of a 3–2–1 pitch, roll, and yaw (θ, ϕ, ψ) rotation sequence. As the spacecraft is assumed to have dimensions much smaller than D, its orbital motions are decoupled from its attitude motions. Therefore, the spacecraft's displacements from the Lagrangian point, x_p, y_p, and z_p, can be assumed to be prescribed.

III. Equations of Motion

The rotations of a rigid body about the body principal axes are governed by Euler's equations. The gravitational gradient torques exerted by the primary bodies are the dominant torques acting on a spacecraft near the Lagrangian points. Other environmental torques, such as the solar radiation torque, can be treated as perturbations. The moments of inertia of the spacecraft about the x_B, y_B, and z_B axes are denoted by J_{xx}, J_{yy}, and J_{zz}, respectively. From previous works, the first order gravity gradient torque exerted by the ith primary body about the rigid body's center of mass can be written as

$$\mathbf{T}_i = \left(3GM_i/R_i^3\right)[(J_{zz} - J_{yy})u_{iyB}u_{izB}\mathbf{i}_B + (J_{xx} - J_{zz})u_{ixB}u_{izB}\mathbf{j}_B + (J_{yy} - J_{xx})u_{ixB}u_{iyB}\mathbf{k}_B] \tag{4}$$

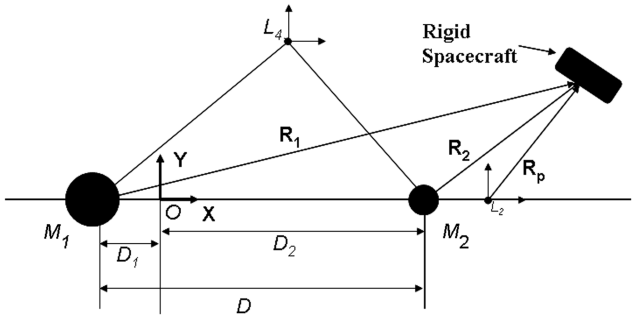

Fig. 1 Geometry of the system.

$$u_{ixB} = [(X_L + x_p \pm D_i)\cos\theta\cos\phi + (Y_L + y_p)\sin\theta\cos\phi - z_p\sin\phi]/R_i \tag{5}$$

$$u_{iyB} = [(X_L + x_p \pm D_i)(\cos\theta\sin\phi\sin\psi - \sin\theta\cos\psi) + (Y_L + y_p)(\sin\theta\sin\phi\sin\psi + \cos\theta\cos\psi) + z_p\cos\phi\sin\psi]/R_i \tag{6}$$

$$u_{izB} = [(X_L + x_p \pm D_i)(\cos\theta\sin\phi\cos\psi + \sin\theta\sin\psi) + (Y_L + y_p)(\sin\theta\sin\phi\cos\psi - \cos\theta\sin\psi) + z_p\cos\phi\cos\psi]/R_i \tag{7}$$

where R_i is the distance from the ith primary mass to the center of mass of the spacecraft. The components of the unit vector along $\mathbf{R}_i$, u_{ixB}, u_{iyB}, and u_{izB}, are expressed in the body frame with the positive sign for $i = 1$ and the negative sign for $i = 2$ in Eqs. (5–7). As working with a set of nondimensional equations is more convenient, a set of dimensionless quantities are defined as follows:

$$\tau = \Omega t, \qquad \hat{\omega}_x = \omega_x/\Omega, \qquad \hat{\omega}_y = \omega_y/\Omega$$
$$\hat{\omega}_z = \omega_z/\Omega, \qquad \hat{u}_{ixB} = u_{ixB}/D, \qquad \hat{u}_{iyB} = u_{iyB}/D \tag{8}$$
$$\hat{u}_{izB} = u_{izB}/D, \qquad \hat{R}_i = R_i/D$$

There are a total of six state variables $(\omega_x, \omega_y, \omega_z, \theta, \phi, \psi)$. Euler's equations and the kinematic differential equations described here are solved together to obtain the complete rotational dynamics of the rigid spacecraft:

$$\hat{\omega}_x' = \frac{(J_{yy} - J_{zz})}{J_{xx}}\left\{\hat{\omega}_y\hat{\omega}_z - 3\left[\frac{(1-\beta)}{\hat{R}_1^3}\hat{u}_{1yB}\hat{u}_{1zB} + \frac{\beta}{\hat{R}_2^3}\hat{u}_{2yB}\hat{u}_{2zB}\right]\right\} \tag{9}$$

$$\hat{\omega}_y' = \frac{(J_{zz} - J_{xx})}{J_{yy}}\left\{\hat{\omega}_x\hat{\omega}_z - 3\left[\frac{(1-\beta)}{\hat{R}_1^3}\hat{u}_{1xB}\hat{u}_{1zB} + \frac{\beta}{\hat{R}_2^3}\hat{u}_{2xB}\hat{u}_{2zB}\right]\right\} \tag{10}$$

$$\hat{\omega}_z' = \frac{(J_{xx} - J_{yy})}{J_{zz}}\left\{\hat{\omega}_x\hat{\omega}_y - 3\left[\frac{(1-\beta)}{\hat{R}_1^3}\hat{u}_{1xB}\hat{u}_{1yB} + \frac{\beta}{\hat{R}_2^3}\hat{u}_{2xB}\hat{u}_{2yB}\right]\right\} \tag{11}$$

$$\begin{bmatrix}\psi'\\ \phi'\\ \theta'\end{bmatrix} = \frac{1}{\cos\phi}\begin{bmatrix}\cos\phi & \sin\phi\sin\psi & \sin\phi\cos\psi\\ 0 & \cos\phi\cos\psi & -\cos\phi\sin\psi\\ 0 & \sin\psi & \cos\psi\end{bmatrix}\begin{bmatrix}\hat{\omega}_x + \sin\phi\\ \hat{\omega}_y - \cos\phi\sin\psi\\ \hat{\omega}_x - \cos\phi\cos\psi\end{bmatrix} \tag{12}$$

Collinear point satellites are usually placed in semistable periodic orbits around the Lagrangian point of interest. While analytical descriptions of the station-keeping orbits usually involve many higher-order terms, a first order approximation is usually sufficient if the orbit is relatively small compared with D. The reference trajectory [5] chosen here is

$$x_p = -A_x\sin w_{xy}\tau \tag{13}$$

$$y_p = -A_y\cos w_{xy}\tau \tag{14}$$

$$z_p = A_z\cos w_z\tau \tag{15}$$

where A_x, A_y, and A_z are the amplitudes of the orbit in the x, y, and z directions, and w_{xy} and w_z are the nondimensional frequencies of the in-plane and out-of-plane motions, respectively. The amplitudes are related such that $A_y = A_z = KA_x$ with K being a constant calculated from the parameters of the three-body system. In this note, the term Lyapunov orbit refers to an orbit solely in the plane of motion of the primary bodies, and the term vertical Lyapunov orbit is used to designate a small 3-D orbit described by Eqs. (13–15) with $w_{xy} = w_z$. A vertical Lyapunov orbit differs from a halo orbit described in literature in that Eqs. (13–15) are obtained from linearized equations of the circular restricted three-body problem.

IV. Attitude Dynamics Near the Collinear Points

A. Linearized Equations

The attitude stability of a rigid body located near the L_1 and L_2 points can be studied using a set of linear equations. Equations (9–11) can be linearized about the equilibrium configuration $\theta_E = \phi_E = \psi_E = 0$ by setting $\hat{Y}_L = 0$ and assuming $\hat{x}_p$, $\hat{y}_p$, and $\hat{z}_p$ to be small. The resulting linear equations for yaw, roll, and pitch, respectively, are

$$\psi'' + (k_1 - 1)\phi' + k_1\psi - 3Ck_1(\hat{y}_p\phi - \hat{z}_p\theta) = 0 \tag{16}$$

$$\phi'' + (1 - k_2)\psi' + (3B + 1)k_2\phi + 3Ck_2(\hat{z}_p - \hat{y}_p\psi) = 0 \tag{17}$$

$$\theta'' + 3Bk_3\theta - 3Ck_3(\hat{z}_p\psi + \hat{y}_p) = 0 \tag{18}$$

$$k_1 = \frac{(J_{zz} - J_{yy})}{J_{xx}}, \qquad k_2 = \frac{(J_{zz} - J_{xx})}{J_{yy}}, \qquad k_3 = \frac{(J_{yy} - J_{xx})}{J_{zz}}$$

where k_1, k_2, k_3 are the inertia ratios. The nondimensional values B and C are defined as

$$B = \frac{(1-\beta)}{\hat{R}_{1L}^3} + \frac{\beta}{\hat{R}_{2L}^3}, \qquad C = \frac{(1-\beta)}{\hat{R}_{1L}^4} + \frac{\beta}{\hat{R}_{2L}^4} \tag{19}$$

Their values are bounded as $|k_s| \leq 1$ for $s = 1, 2, 3$. For collinear points of the sun–Earth system, $(B_{L1}, C_{L1}) = (4.06, 302.89)$, and $(B_{L2}, C_{L2}) = (3.94, 296.89)$. By comparison the values of B and C for the Earth–moon L_1 and L_2 are $(B_{L1}, C_{L1}) = (5.15, 21.51)$, and $(B_{L2}, C_{L2}) = (3.19, 15.85)$. The frequencies of the attitude motions exactly at the collinear points are found to be

$$\omega_1 = \sqrt{\frac{k_1k_2 + 3Bk_2 + 1 - \sqrt{(k_1k_2 + 3Bk_2 + 1)^2 - 4(3B+1)k_1k_2}}{2}} \tag{20}$$

$$\omega_2 = \sqrt{\frac{k_1k_2 + 3Bk_2 + 1 + \sqrt{(k_1k_2 + 3Bk_2 + 1)^2 - 4(3B+1)k_1k_2}}{2}} \tag{21}$$

$$\omega_{\text{pitch}} = \sqrt{3Bk_3} \tag{22}$$

with ω_{pitch} being the pitch frequency and ω_1 and ω_2 being the two roll-yaw frequencies. The linear attitude stability of the spacecraft depends on the inertia ratios and the constant B. Robinson [3] determined the stability conditions and the permissible range of inertia ratios, constructed a linear attitude stability chart for a body located exactly at L_2, and found that the stability conditions of a L_2 rigid body are identical to those for a geocentric satellite.

B. Resonant Motion of a Spacecraft in Planar Lyapunov Orbits

When the rigid spacecraft occupies a Lyapunov or vertical Lyapunov orbit, the gravity gradient torques it experiences are functions of the amplitudes and frequencies of the orbits as well as its inertia ratios. Analysis of the linear attitude equations showed that for a spacecraft traveling in a Lyapunov orbit, certain critical values of k_1, k_2, and k_3 can trigger large attitude motions. Eq. (18) can be solved analytically to yield

$$\theta(\tau) = \left(\theta_o - \frac{3Ck_3\hat{A}_y}{\omega_{\text{pitch}}^2 - w_{xy}^2}\right)\cos\omega_{\text{pitch}}\tau + \frac{\theta_0'}{\omega_{\text{pitch}}}\sin\omega_{\text{pitch}}\tau + \frac{3Ck_3\hat{A}_y}{\omega_{\text{pitch}}^2 - w_{xy}^2}\cos w_{xy}\tau \tag{23}$$

As $|\omega_{\text{pitch}} - w_{xy}|$ approaches 0 or $k_3 \to w_{xy}^2/3B$, the linear solution $\theta(\tau)$ will increase rapidly and violate the small angles assumption, requiring a nonlinear analysis of the rotational dynamics. From Eq. (23) it can be seem the linear pitch resonance condition is independent of the size of the orbit. At the sun–Earth L_2, $k_{3\text{critical}} \approx 0.3579$ with $B = 3.94$ and $w_{xy} = 2.057$, while $k_{3\text{critical}} \approx 0.364$ at the Earth–moon L_2 with $B = 3.19$ and $w_{xy} = 1.868$. Figure 2 compares the amplitude of pitch motions for spacecraft with and without the critical k_3.

It can be shown that roll-yaw resonance occurs when $|\omega_2 - \omega_1| = w_{xy}$. The resonance curve $f(k_1, k_2)$ for a rigid collinear point spacecraft can be derived by substituting Eqs. (20) and (21) into the resonance condition to yield

$$f(k_1, k_2) = k_1k_2 + 3Bk_2 + 1 - 2\sqrt{(3B+1)k_1k_2} - w_{xy}^2 = 0 \tag{24}$$

The resulting roll-yaw resonance curve can be found in the Lagrange region of a linear stability diagram and extends upward into the unstable regions, and adds an additional restriction on the configuration of the spacecraft. An example of the modified stability chart for the sun–Earth L_2 are shown in Fig. 3. At other collinear points such as the Earth–moon L_2, the stability chart and the resonant curve appear to be the same graphically but gives different values. Resonant roll and yaw motions should not be a practical problem encountered on short terms missions because of the long periods of roll and yaw rotations and the slow growth of the amplitude even at resonance.

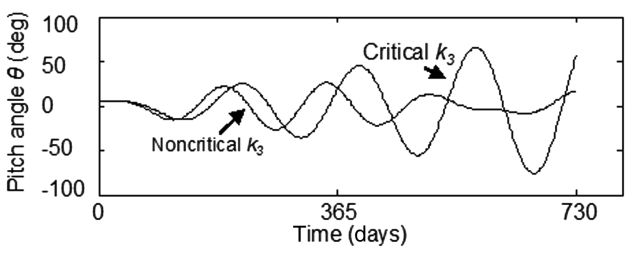

Fig. 2 Pitch resonance of lost solar panel orbiting the sun–Earth L_2.

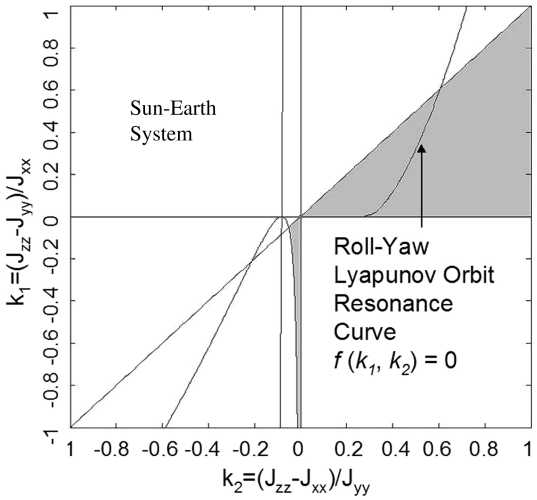

Fig. 3 Gravity gradient stability plot for L_2 bodies.

C. Attitude Motions of a Spacecraft in Periodic Orbits

The nonlinear attitude dynamics of a spacecraft traveling in the two different types of reference orbits are investigated in this section. Using Robinson's linear stability diagram as a starting point, the goal of this study is to determine if a spacecraft that is gravity gradient stable at L_2 has similar stability characteristics when it is traveling in Lyapunov and vertical Lyapunov orbits of different sizes. To this end Euler's equations given by Eqs. (9–11) are numerically solved together with the kinematics equation Eq. (12), with the trajectory of the periodic orbit given by Eqs. (13–15). The inertia ratios k_1, k_2, and k_3 of the spacecraft belong in the Lagrangian region of linear stability diagram. Representative results shown in Figs. 4 and 5 for the spacecraft traveling in the different reference orbits around the sun–Earth L_2. In Fig. 4, it can be seen that greater pitch and yaw motions are encountered as the size of the Lyapunov orbit increases from $A_x = 1000$ km to $A_x = 100,000$ km, while roll oscillations are not much affected as there is no orbital movement in the z-direction. The frequencies of the angular rotations are not affected much by the size of the orbit.

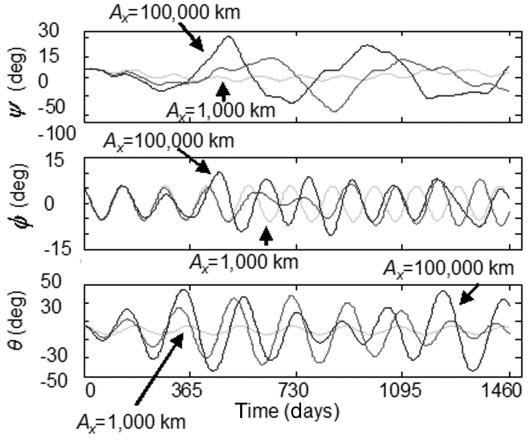

Fig. 4 Lagrange region rigid body in Lyapunov orbit around sun–Earth L_2.

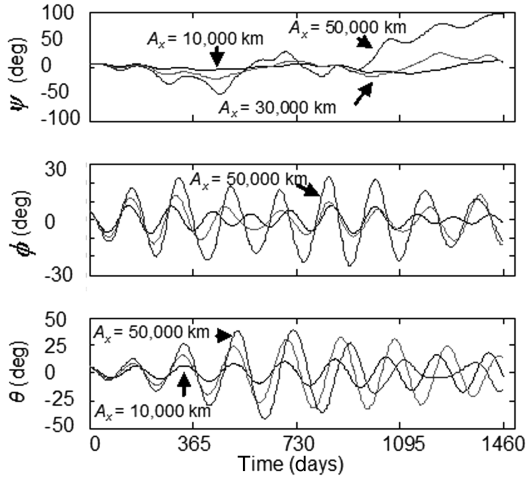

Fig. 5 Lagrange region body in vertical Lyapunov orbit around sun–Earth L_2.

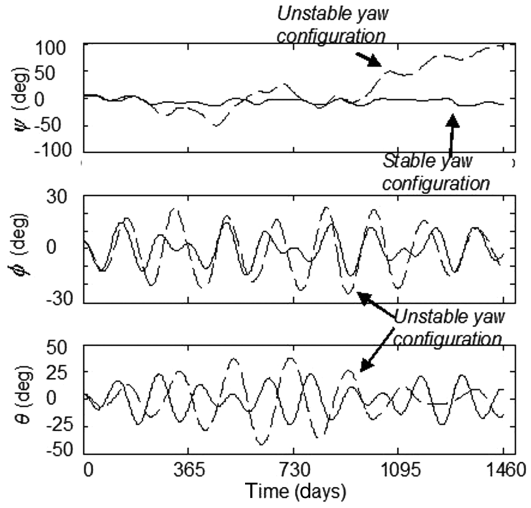

Fig. 6 Rigid body with yaw stable configuration in $A_x = 50,000$ km vertical Lyapunov orbit.

After performing a number of numerical trials for the vertical Lyapunov orbit cases, it was observed that attitude motions are stable for the $A_x = 10,000$ km and $A_x = 30,000$ km cases, while yaw instability was detected when $A_x = 50,000$ km, as can be seen in Fig. 5. It was also observed that yaw motions are bounded for the largest tested orbit if the three rotational inertia are related such that $J_{yy} = 3.29J_{xx}$, and $J_{zz} = 3.3J_{xx}$. Figure 6 compares the attitude motions of a spacecraft with the yaw stable configuration described above to the results obtained in Fig. 5. The results presented here are obtained numerically, and the underlying dynamics behind the detected yaw instability and the proposed remedy is unclear at the moment. The instability is suspected to be another resonance phenomenon similar to those observed in the planar orbit cases and can likely be evaluated using techniques such as Floquet theory.

V. Attitude Stability at the Triangular Points

A. Attitude Stability at the Sun–Earth L_4

The nondimensional coordinates of the triangular Lagrangian points in the primary frame are given by $\hat{X}_L = 1/2 - \beta$ and $\hat{Y}_L = \pm\sqrt{3}/2$, with the positive sign for L_4, the negative sign for L_5, and $\beta = M_2/(M_1 + M_2)$. Setting all the time derivatives, along with x_p, y_p, and z_p, to zero, Eqs. (9–11), the equilibrium equations of a rigid triangular point spacecraft can be satisfied by $\tan 2\theta_E = \mp\sqrt{3}(1 - 2\beta)$ and $\phi_E = \psi_E = 0$. It is not necessary to consider spacecraft translational motions as the triangular points are stable. Eqs. (9–11) can be linearized about $(\theta_E, 0, 0)$ to produce

$$\psi'' + (k_1 - 1)\phi' + Lk_1\psi = 0 \tag{25}$$

$$\phi'' + (1 - k_2)\psi' + Mk_2\phi = 0 \tag{26}$$

$$\theta'' + (2M - 5)k_3\theta = 0 \tag{27}$$

$$L = \frac{5}{2} \pm \frac{3}{4}\sqrt{1 + a^2} \tag{28}$$

$$M = \frac{5}{2} \mp \frac{3}{4}\sqrt{1 + a^2} \tag{29}$$

$$a = \mp \tan 2\theta_E \tag{30}$$

L and M are both positive definite, and the positive sign corresponds to the first equilibrium configuration (θ_{1E}, 0 ,0), while the negative sign is for the second configuration (θ_{2E}, 0 ,0). Figures 7a and 7b are obtained by combining the values of L and M calculated for the two

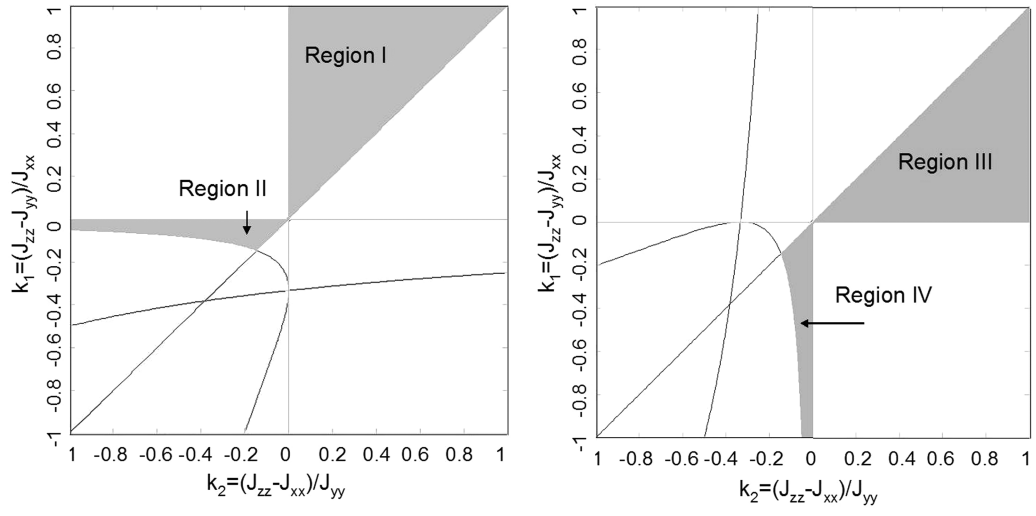

a) b)

Fig. 7 a) Gravity gradient stability plot near θ_{1E}. b) Gravity gradient stability plot near θ_{2E}.

equilibrium configurations together with the linear stability conditions derived by Robinson [3]. The two figures illustrate the regions of stability near the first and second equilibrium configurations. It should be noted that the stability plot near θ_{2E} is similar to those obtained for collinear point and geocentric satellites. The shaded regions I and II in Fig. 7a represent the stable regions near the first equilibrium. Region I encompasses bodies with $J_{zz} > J_{xx} > J_{yy}$, while bodies in the much smaller region II must have $J_{xx} > J_{yy} > J_{zz}$. Similarly, regions III and IV in Fig. 7b represent the stable regions near the second equilibrium. Bodies with $J_{zz} > J_{yy} > J_{xx}$ belong in region III, and in the DeBra–Delp-like region IV, $J_{yy} > J_{xx} > J_{zz}$ is necessary, but not sufficient. The structures of regions I and III reflect Robinson's pitch stability condition, which requires $k_3 < 0$ or $k_1 > k_2$ near θ_{1E} and the opposite near θ_{2E}. Regions II and IV are similarly mirrored. Overall, the stable regions about the two equilibrium configurations appear to be mirrored about the $k_1 = k_2$ line, implying that a gravity gradient stable orientation for one equilibrium configuration is unstable about the other equilibrium. The physical implications can be illustrated with a simple example. To satisfy the conditions for pitch stability near θ_{1E}, the long axis of a rectangular prism must point along y_B, while its intermediate axis points along x_B, and the short axis points along z_B. Near θ_{2E}, the same rectangular prism must have its long axis along x_B, intermediate axis along y_B, and the short axis about z_B.

VI. Conclusions

The effects of spacecraft orbital motion on its attitude dynamics in the vicinity of a collinear Lagrangian point are briefly investigated. Previous research established the gravity gradient stability characteristics of a spacecraft stationed at a collinear point, and the work here extends those results to spacecraft in small Lyapunov and vertical Lyapunov orbits. Pitch, roll, and yaw motions are stable for a spacecraft in a small Lyapunov orbit, and the amplitude of the attitude motions depend on the size of the orbit. Similar results are also obtained with spacecraft in smaller vertical Lyapunov orbits, while yaw instability is encountered at larger orbits. This instability can be countered by changing the shape of the spacecraft. Resonant attitude motion can occur if the spacecraft has inertia ratios such that its natural frequencies and the frequency of its Lyapunov orbit satisfy certain conditions. At the triangular points, two equilibrium pitch angles are found for a particular primary body's mass ratio. Linearizing Euler's equations about the two equilibrium configurations, it is found that the natural frequencies and the stability of the attitude motions are different for the two configurations. The stable regions on the linear stability plot are different for each equilibrium position, such that a spacecraft designed to be stable at one stationary configuration is unstable at the other equilibrium configuration.

References

[1] Kane, T. R., and Marsh, E. L., "Attitude Stability of a Symmetric Satellite at the Equilibrium Points in the Restricted Three-Body Problem," *Celestial Mechanics*, Vol. 4, No. 1, Sept. 1971, pp. 78–90. doi:10.1007/BF01230323

[2] Robinson, W. J., "The Restricted Problem of Three Bodies with Rigid Dumb-Bell Satellite," *Celestial Mechanics*, Vol. 8, No. 2, Sept. 1973, pp. 323–330. doi:10.1007/BF01231434

[3] Robinson, W. J., "Attitude Stability of a Rigid Body Placed at an Equilibrium Point in the Restricted Problem of Three Bodies," *Celestial Mechanics*, Vol. 10, No. 1, Aug. 1974, pp. 17–33. doi:10.1007/BF01261876

[4] Misra, A. K., and Bellerose, J., "Dynamics of a Tethered System Near the Earth–Moon Lagrangian Point," *Advances in the Astronautical Sciences*, AAS 01-328, Vol. 109, Pt. 1, Univelt, Incorporated, San Diego, CA, 2001, pp. 415–435.

[5] Wie, B., *Space Vehicle Dynamics and Control*, AIAA Education Series, AIAA, Reston, VA, 1998, pp. 240–256.